



Published in final edited form as:

*Proteomics*. 2015 January ; 15(0): 462–473. doi:10.1002/pmic.201400154.

## Effects of MEK inhibitors GSK1120212 and PD0325901 *in vivo* using 10-plex quantitative proteomics and phosphoproteomics

Joao A. Paulo<sup>1,\*,#</sup>, Fiona E. McAllister<sup>1,\*</sup>, Robert A. Everley<sup>1</sup>, Sean A. Beausoleil<sup>2</sup>, Alexander S. Banks<sup>3</sup>, and Steven P. Gygi<sup>1,#</sup>

<sup>1</sup>Department of Cell Biology, Harvard Medical School, Boston, Massachusetts 02115, USA

<sup>2</sup>Cell Signaling Technologies, Danvers, MA 01923, USA

<sup>3</sup>Brigham and Women's Hospital, Harvard Medical School, Boston, Massachusetts 02115, USA

### Abstract

Multiplexed isobaric tag-based quantitative proteomics and phosphoproteomics strategies can comprehensively analyze drug treatments effects on biological systems. Given the role of MEK signaling in cancer and MAPK-dependent diseases, we sought to determine if this pathway could be inhibited safely by examining the downstream molecular consequences. We used a series of TMT10-plex experiments to analyze the effect of two MEK inhibitors (GSK1120212 and PD0325901) on three tissues (kidney, liver, and pancreas) from nine mice. We quantified ~6000 proteins in each tissue, but significant protein level alterations were minimal with inhibitor treatment. Of particular interest was kidney tissue, as edema is an adverse effect of these inhibitors. From kidney tissue, we enriched phosphopeptides using titanium dioxide (TiO<sub>2</sub>) and quantified 10,562 phosphorylation events. Further analysis by phosphotyrosine (pY) peptide immunoprecipitation quantified an additional 592 phosphorylation events. Phosphorylation motif analysis revealed that the inhibitors decreased phosphorylation levels of PxSP and SP sites, consistent with ERK inhibition. The MEK inhibitors had the greatest decrease on the phosphorylation of two proteins, Barttin and Slc12a3, which have roles in ion transport and fluid balance. Further studies will provide insight into the effect of these MEK inhibitors with respect to edema and other adverse events in mouse models and human patients.

### Keywords

Phosphoproteomics; multiplexing; 10-plex TMT; MEK inhibitors; Barttin; Bartter Syndrome; GSK1120212; PD0325901

---

<sup>#</sup>Corresponding authors: Steven P. Gygi, Department of Cell Biology, 240 Longwood Ave. Harvard Medical School, Boston, Massachusetts 02115, USA, sgygi@hms.harvard.edu. Joao A. Paulo, Department of Cell Biology, 240 Longwood Ave. Harvard Medical School, Boston, Massachusetts 02115, USA, joao\_paulo@hms.harvard.edu.

<sup>\*</sup>These authors contributed equally

### Conflicts of interest

The authors acknowledge no conflict of interest.

## 1. Introduction

Multiplexing strategies are widely applicable to mass spectrometry-based quantitative proteomic and phosphoproteomic analyses. Such strategies improve the efficiency of data collection resulting in comprehensive and robust datasets. With the advent of isobaric tagging [1–3], virtually any protein sample may be labeled and subsequently quantified, with the present limitation being the number of available isobaric tags.

MEK inhibitors typically act on the mitogen-activated protein kinase kinase enzymes, MEK1 and MEK2, in the Ras/Raf/MEK/ERK signaling pathway. Specifically, when MEK is inhibited, cell proliferation is blocked and apoptosis is induced, therefore this class of drugs shows promise in cancer research [4], in particular for melanoma [5], and may be applied to other MAP kinase-dependent diseases [6, 7]. We chose to investigate the effects of two different MEK inhibitor drugs, GSK1120212 (Trametinib/Mekinist) and PD0325901 *in vivo*. Multiple MEK inhibitors have failed to show significant efficacy as monotherapy in clinical trials, with common on-target adverse events including skin rash, edema, nausea, and diarrhea [8]. PD0325901, had promising preclinical, phase I and phase II clinical trial results in the treatment of melanoma, but development as a monotherapy was abandoned in 2008 due to adverse side effects [9, 10]. Specifically, PD0325901 was discontinued because of toxicities associated with intolerable drug levels passing the blood barriers of the retina and central nervous system [11, 12]. However, the use of GSK1120212 avoided such toxicities and the drug recently became the first FDA-approved MEK inhibitor to be used as a cancer therapy [13].

As with many drugs undergoing clinical trials, the MEK inhibitors GSK1120212 and PD0325901 have shown adverse events in study patients. One such common event of both inhibitors is edema [5, 9, 10, 14], which is the abnormal accumulation of fluid in the interstitium due to ion imbalance by the kidney, often linked to retention of water [15]. In the present study, we investigate the effects of GSK1120212 and PD0325901 in ob/ob mutant mice, an animal model for obesity and insulin resistance [16, 17]. These leptin-deficient mice are indistinguishable from littermates at birth, but eat excessively and quickly to become obese [18]. ob/ob mice exhibit elevated MAP kinase activity [19], which is attributed to a chronic low-grade inflammatory state. We exploited the elevated MAP kinase activity in these mice so as to observe better the proteomic and phosphoproteomic alterations in response to the drugs, which may be too subtle to detect in wildtype mice. The ob/ob mouse model is well characterized and in our study may reflect the effects of GSK1120212 and PD0325901 in patients with elevated MEK/ERK signaling but without tumor burden. In these mice, inhibitors of the MEK/ERK pathway (e.g., GSK1120212 and PD0325901) are pharmacologically well tolerated and improve glucose homeostasis. However, signs of edema have been observed in these mice (A. Banks, unpublished data), as in human clinical trials, as an adverse reaction to drug treatment [9, 10, 13].

We aimed to understand better the mechanisms underlying the adverse effects of GSK1120212 and PD0325901 and subsequent development of edema. To this end, we investigated protein expression differences in the kidney, liver and pancreas of ob/ob mice treated with these MEK inhibitors, using 9 mice in a multiplexed 3x3+1 approach. This

strategy allows for 3 controls, 3 GSK1120212-treated mice, 3 PD0325901-treated mice, and 1 mixed tissue sample to compare across the different 10-plex experiments. We subsequently focused on the kidney tissue in which we performed total phosphopeptide and phosphotyrosine enrichment again using TMT 10-plex labeling and associated fractionation. Applying the approach outlined herein to other systems will permit the global proteome and phosphoproteome analysis of virtually any sample type or number.

## 2. Materials and Methods

### 2.1 Materials

Tandem mass tag (TMT) isobaric reagents were from Thermo Scientific (Rockford, IL). Water and organic solvents were from J.T. Baker (Center Valley, PA). GSK1120212 and PD0325901 were from Selleckchem (Houston, TX). Titanosphere TiO<sub>2</sub> 5 μm particles were from GL Biosciences, (Tokyo, Japan). Phosphotyrosine (pY) 1000 antibody was from Cell Signaling Technology (Beverly, MA). Unless otherwise noted, all other chemicals were from Sigma-Aldrich (St. Louis, MO).

### 2.2 Mice

All animal experiments were performed according to procedures approved by Beth Israel Deaconess Medical Center's Institutional Animal Care and Use Committee. The mice (strain: B6.Cg-Lepob/J from Jackson Labs) were 8 weeks old when administered inhibitor or vehicle by once daily oral gavage for 5 days. Doses in mice (GSK1120212, 3 mg/kg in DMSO; PD0325901, 10 mg/kg in DMSO) were diluted in 15% Cremophor EL/ 82% saline/ 3% drug or DMSO were comparable to that given in human clinical trials [5, 9, 10, 14]. Kidneys, livers, and pancreata from nine mice were dissected and flash frozen in liquid nitrogen.

### 2.3 Tissue homogenization and cell lysis

Tissues were homogenized in lysis buffer (2.5% SDS, 150 mM NaCl, 50 mM HEPES pH 8.5, 1X Roche Protease Inhibitors, 1X Roche PhosphoStop phosphatase inhibitors) at a tissue concentration of approximately 10–15 mg/mL using a polytron tissue grinder. Following homogenization, the tissue was incubated at 37°C for 30 min for reduction of disulfide bonds using 5 mM TCEP. Cysteines were alkylated with 15 mM iodoacetamide via a 30 min incubation at room temperature in the dark. Excess iodoacetamide was quenched with 5 mM DTT for 15 min at room temperature in the dark.

Chloroform-methanol precipitation of proteins was performed prior to protease digestion [20]. In brief, four parts neat methanol was added to each sample and vortexed, one part chloroform was added to the sample and vortexed, and three parts water was added to the sample and vortexed. The sample was centrifuged at 4,000 RPM for 15 min at room temperature and subsequently washed twice with 100% methanol.

Samples were resuspended in a small volume of 8 M urea, 50 mM HEPES pH 8.5 to aid dissolution and then diluted to 1 M urea, 50 mM HEPES pH 8.5 for digestion. Protein concentrations were determined using the BCA assay. For each of the 27 samples, 10 mg of

protein was digested at 37°C for 3 hrs with LysC protease at a 1:100 protease-to-protein ratio. Trypsin was then added at a 1:100 protease-to-protein ratio and incubated overnight at 37°C. This reaction was then quenched with 1% formic acid, subjected to C18 solid-phase extraction (SPE) (Sep-Pak, Waters) and subsequently vacuum-centrifuged to near-dryness. Peptides were resuspended in 100 mM HEPES pH 8.5 and peptide concentration was determined using the microBCA assay (Pierce). From each sample, 50 µg of peptide was removed for protein level analysis and the remaining amount of the kidney tissue digests were used for phosphoprotein enrichment, while those of the liver and pancreas were stored for future use.

## 2.4 Phosphopeptide enrichment

Phosphopeptides were enriched using a method based on that of Kettenbach and Gerber [21]. In brief, Titanosphere TiO<sub>2</sub> 5 µm particles (GL Biosciences, Tokyo, Japan) were washed three times with 2 M lactic acid/ 50% acetonitrile. Peptides were resuspended in 2.5 mL of 2 M lactic acid/50 % acetonitrile. For ~10 mg of peptide digest, 40 mg beads were added and incubated with gentle rotation for 1 hr at room temperature. Beads were washed twice with 2.5 mL of 2 M lactic acid/ 50% acetonitrile, then twice with 2.5 mL of 50% acetonitrile/ 0.1% TFA, and finally twice with 2.5 mL of 25% acetonitrile/ 0.1% TFA. Enriched phosphopeptides were eluted twice with 500 µL of 50 mM K<sub>2</sub>HPO<sub>4</sub> pH 10 and vacuum centrifuged to dryness.

## 2.5 Tandem mass tag labeling

In preparation for TMT labeling, desalted peptides (both for protein expression and phosphopeptide level analyses) were dissolved in 100 mM HEPES, pH 8.5. Peptide concentrations were determined using the microBCA assay. Approximately 50 µg of peptides from each tissue sample were labeled with TMT reagent. The tissues (kidney, liver, pancreas) from each mouse were labeled with the same TMT tag (i.e., the kidney, liver, and pancreas from mouse 1 were labeled with TMT126, etc.). The samples labeled with TMT131 were mixtures of 3.7µg of peptide from each of the 27 individual samples. These mixed samples were prepared separately for total proteome and phosphoproteome analyses.

TMT reagents (0.8 mg) were dissolved in anhydrous acetonitrile (40 µL) of which 10 µL was added to the peptides (resuspended in 70 µL of 100 mM HEPES, pH 8.5) along with 20 µL of acetonitrile to achieve a final acetonitrile concentration of 30% (v/v). Following incubation at room temperature for 1 hr, the reaction was quenched with hydroxylamine to a final concentration of 0.3% (v/v). The TMT-labeled samples were combined at a 1:1:1:1:1:1:1:1:1 ratio. The sample was acidified, vacuum centrifuged to near dryness and subjected to C18 solid-phase extraction (SPE) (Sep-Pak, Waters).

## 2.6 Enrichment of phosphotyrosine (pY)-containing peptides

Following TMT labeling and combining, we subjected a titanium-enriched fraction of mouse kidney tissue digest to pY enrichment. The sample was reconstituted in 1.8 mL of immunoaffinity purification (IAP) buffer (50 mM MOPS pH 7.2, 10 mM sodium phosphate, 50 mM NaCl) and 100 µL of phosphotyrosine (pY) 1000 bead slurry (Cell Signaling Technology, Beverly, MA) was added and rotated for 45 min at 4 °C. The tube was then

centrifuged for 2 min at 1500 rpm and the supernatant was removed. This supernatant consisted of enriched phosphopeptides (mainly pT and pS) which did not bind the pY beads. This sample was fractionated using BpRP chromatography as described below. The beads were washed twice with IAP buffer and thrice with water. Phosphotyrosine peptides were eluted by incubation in 55  $\mu$ L of 0.15 % TFA for 10 min. After centrifugation, the supernatant containing pY peptides was removed and the beads were washed with 45  $\mu$ L of 0.15 % TFA. This supernatant was added to the eluted phosphopeptide solution for a total volume of 100  $\mu$ L. The pY peptide-containing solution was passed through a 0.2  $\mu$ m centrifugal PTFE (polytetrafluoroethylene) filter (Millipore Corporation, Billerica, MA) to remove unwanted beads. The filtered solution was then StageTipped for desalting prior to mass spectrometry analysis. The final sample was reconstituted in 5  $\mu$ L of 5% formic acid in water and 4  $\mu$ L were analyzed on the mass spectrometer (as described below).

## 2.7 Offline basic pH reversed-phase (BpRP) fractionation

Samples were separated using basic pH reversed-phase HPLC for protein-level and total phosphoproteome analysis, following TMT labeling and combining of the isobarically-labeled fractions. Using an Agilent 1100 quaternary pump equipped with a degasser and a photodiode array (PDA) detector (set at 220 and 280-nm wavelength) from ThermoFisher (Waltham, MA), a 50 min linear gradient from 5% to 35% acetonitrile in 10mM ammonium bicarbonate pH 8 at a flow rate of 0.8 mL/min with an Agilent 300Extend C18 column (5  $\mu$ m particles, 4.6 mm ID and 220 mm in length) separated the peptide mixture into a total of 96 fractions which were consolidated into 12 using a checkerboard pattern. Samples were subsequently acidified with 1% formic acid and vacuum centrifuged to near dryness. Each fraction was desalted via StageTip, dried via vacuum centrifugation, and reconstituted in 5% acetonitrile, 5% formic acid for LC-MS/MS processing.

## 2.8 Liquid chromatography and tandem mass spectrometry

Our mass spectrometry data were collected using an Orbitrap Elite mass spectrometer (Thermo Fisher Scientific, San Jose, CA) coupled with a Proxeon EASY-nLC II liquid chromatography (LC) pump (Thermo Fisher Scientific). Peptides were separated on a 100  $\mu$ m inner diameter microcapillary column packed with 0.5 cm of Magic C4 resin (5  $\mu$ m, 100  $\text{\AA}$ , Michrom Bioresources) followed by 20 cm of Maccel C18 resin (3  $\mu$ m, 200  $\text{\AA}$ , Nest Group). For each analysis, we loaded approximately 1  $\mu$ g onto the column.

Peptides were separated using a 3 hr gradient of 6 to 30% acetonitrile in 0.125% formic acid with a flow rate of 300 nL/min. Each analysis used an MS<sup>3</sup>-based TMT method [22] [23]. The scan sequence began with an MS<sup>1</sup> spectrum (Orbitrap analysis, resolution 60,000, 300 1500 Th, automatic gain control (AGC) target  $1 \times 10^6$ , maximum injection time 150 ms). The top ten precursors were then selected for MS<sup>2</sup>/MS<sup>3</sup> analysis. MS<sup>2</sup> analysis consisted of collision-induced dissociation (CID), quadrupole ion trap analysis, automatic gain control (AGC)  $2 \times 10^3$ , NCE (normalized collision energy) 35, q-value 0.25, maximum injection time 100 ms). Following acquisition of each MS<sup>2</sup> spectrum, we collected an MS<sup>3</sup> spectrum using our recently described method in which multiple MS<sup>2</sup> fragment ions are captured in the MS<sup>3</sup> precursor population using isolation waveforms with multiple frequency notches [22]. MS<sup>3</sup> precursors were fragmented by HCD and analyzed using the Orbitrap (NCE 50,

Max AGC  $1.5 \times 10^5$ , maximum injection time 250 ms, isolation specificity 0.8 Th, resolution was 30,000 at 400 Th).

## 2.9 Data analysis

Mass spectra were processed using a Sequest-based in-house software pipeline. MS spectra were converted to mzXML using a modified version of ReAdW.exe. Database searching included all entries from the mouse Uniprot database (August 10, 2011), which was concatenated with a reverse database composed of all protein sequences in reversed order. Searches were performed using a 50 ppm precursor ion tolerance for total protein level analysis and 20 ppm for phosphopeptide analysis [23, 24]. Product ion tolerance was set to 1 Da. TMT tags on lysine residues and peptide N termini (+229.1629 Da) and carbamidomethylation of cysteine residues (+57.0215 Da) were set as static modifications, while oxidation of methionine residues (+15.9949 Da) was set as a variable modification. For phosphorylation analysis, +79.9663 Da on serine, threonine, and tyrosine was also set as a variable modification.

Peptide spectral matches (PSMs) were filtered to a 1% FDR [24, 25]. PSM filtering was performed using linear discriminant analysis, as described previously [26], while considering the following parameters: XCorr, Cn, missed cleavages, peptide length, charge state, and precursor mass accuracy. For TMT-based reporter ion quantitation, we extracted the signal-to-noise (S/N) ratio for each TMT channel and found the closest matching centroid to the expected mass of the TMT reporter ion.

The search space for each reporter ion was limited to a range of 0.002 Th to prevent overlap between the isobaric reporter ions. For protein-level comparisons, peptide-spectral matches were identified, quantified, and collapsed to a 1% FDR and then collapsed further to a final protein-level FDR of 1%. Furthermore, protein assembly was guided by principles of parsimony to produce the smallest set of proteins necessary to account for all observed peptides.

Proteins and phosphorylation sites were quantified by summing reporter ion counts across all matching PSMs using in-house software, as described previously [26]. Briefly, a 0.002 Th window around the theoretical m/z of each reporter ion (126, 127N, 127C, 128N, 128C, 129N, 129C, 130N, 130C, 131) was scanned for ions, and the maximum intensity nearest the theoretical m/z was used. PSMs with poor quality, MS<sup>3</sup> spectra with more than seven TMT channels missing, less than 100 TMT reporter summed signal to noise ratio, or no MS<sup>3</sup> spectra at all were excluded from quantitation [27]. Protein quantitation values were exported for further analysis in Excel, Matlab or Mathematica. Hierarchical clustering and unsupervised K-means clustering were performed using Matlab.

For both protein and phosphorylation site quantitation, values for each reporter ion channel were summed across all quantified peptides and normalized assuming equal protein loading across all 10 samples. One-way ANOVA was then used to identify proteins that were differentially expressed across mouse treatments and the method of Benjamini and Hochberg was subsequently applied to control for multiple testing error [28]. A Benjamini-Hochberg-corrected p-value < 0.05 was considered statistically significant. Data were

normalized to the TMT131 channel (separately for the total protein and phosphoprotein data) by dividing the summed signal-to-noise for each protein in each channel by the corresponding value of the 131 channel to compare across different tissue data sets.

## 2.10 Phosphopeptide motif analysis

For the phosphorylation dataset, site localization was evaluated via AScore [29]. Sites with an AScore >13 were analyzed further using the motif-x algorithm [30] (<http://motif-x.med.harvard.edu>). Sequences were centered at the phosphorylated residue and extended six amino acids on each side, thereby giving a length of 13 amino acids for each phosphorylation site. The minimum reported number of occurrences for a given motif was set at 20 and only motifs with a score of >6 were reported. Sequence logos were automatically generated by Weblogo [31].

## 2.11 Data access

RAW files will be made available upon request. Supplementary tables are available on-line providing protein names, TMT signal-to-noise values, and p-values from ANOVA for the kidney (Supplemental Table 1), liver (Supplemental Table 2), and pancreas (Supplemental Table 3) samples. In addition, Supplemental Table 4 provides additional data on the kidney phosphopeptide experiment including the sequence of phosphorylated motif and the ASCORE.

## 3. Results

### 3.1 The proteomes of mice treated with either GSK1120212 or PD0325901 showed minimal alterations when compared to vehicle-treated controls

Our strategy allowed for three controls, three GSK1120212-treated mice, three PD0325901-treated mice, and one mixed sample to be analyzed in a single TMT10-plex experiment (Figure 1A). We subsequently focused on kidney tissue in which two additional experiments were performed - general phosphorylation analysis and phosphotyrosine analysis (Figure 1B). We first examined protein level changes, identifying more than 7900 proteins among the three tissues. Individually, we quantified 5908 proteins in kidney, 5019 in liver, and 5644 in pancreas (Figure 2A).

Histograms of the  $\log_2$ -transformed fold changes of each inhibitor-to-vehicle ratio showed little variation among the 3 tissues (Figure 2B). We tested for statistical significance using a one-way ANOVA and corrected for multiple testing of proteins in each tissue using the post-hoc Benjamini-Hochberg method [28]. With these criteria, we did not identify significantly changing proteins following treatment with either drug in either in the kidney or liver. In the pancreas, nine marginally significant (p-value<0.05, but >0.04) proteins were identified (Supplemental Figure 1). Of potential interest include three proteins, which demonstrated decreased abundance upon treatment with PD0325901: chymotrypsinogen B, kallikrein-1, and pancreatic lipase-related protein 1, all which are commonly identified in pancreatic fluid [32]. Similarly, Vamp2 and Vamp8 levels also decreased with PD0325901. These two proteins were generally associated with zymogen granules, the vesicles in which pancreatic proenzymes were secreted [33]. Thus, the enzymatic transport mechanism and/or

production of these pancreatic enzymes may be compromised upon treatment with PD0325901, but the analogous effect of GSK1120212 was less potent and merit further study.

Moreover, hierarchical clustering by protein expression resulted in the heat map shown in Supplemental Figure 2. Tissues clustered together as expected, but treatments did not always cluster. These results emphasize that few significant changes at the protein expression level were induced by the kinase inhibitors over the 5 day treatment. As such, we investigated cellular signaling via phosphoproteomic analysis, in which alterations would be expected on a shorter time frame.

### 3.2 Phosphopeptide enrichment revealed significant differences in the phosphorylation levels of certain proteins resulting from MEK inhibitor treatment

Inhibition of MEK kinases would be expected to alter protein phosphorylation and signal transduction cascades. As very few changes in protein abundance were noted, we increased the depth of our analysis by investigating the phosphorylation level alterations. As we were interested in proteins involved in the clinical adverse effect of edema, we focused the phosphoproteomic analysis on the kidney samples. We measured changes in phosphorylation across 10,562 sites in kidney (Figure 3A).

As with the protein level data, we tested statistical significance using ANOVA, and set a significance threshold  $p$ -value  $<0.05$ . Using only those sites with a significant difference, we performed K-means clustering and subsequently gene ontology analysis on the clusters (Figure 3B). It followed that the two clusters of most interest were those in which both inhibitors caused either an increase (top cluster; Figure 3B) or a decrease (bottom cluster; Figure 3B) in phosphorylation. The major gene ontology (GO) categories for the cluster with decreased phosphorylation upon inhibitor treatment were cytoskeletal and actin binding. Among the proteins with the greatest decrease in phosphorylation were BSND (Bartter syndrome with sensorineural deafness, Barttin), Ahnak (Neuroblast differentiation-associated protein), Synm (synemin, intermediate filament protein), Flna (Filamin A), and Lsp1 (Lymphocyte-specific protein 1). In contrast, the major GO categories for the cluster demonstrating increased phosphorylation upon inhibitor treatment were ion transport and plasma membrane. Two proteins demonstrating high fold changes in phosphorylation in this cluster included Trpv5 (Transient receptor potential cation channel subfamily V member) and Slc12a3/NCC (sodium-chloride symporter/Na-Cl Cotransporter), which are associated in kidney-related Barttin's syndrome [34]. Focusing on these two clusters, we used motif-x [30, 35] to determine if any phosphorylation motifs were present in the identified phosphopeptides (Figure 3B). The cluster representing decreased phosphorylation showed PxSP and SP as having 37% and 26% enrichment, respectively. In contrast, in the cluster with increased phosphorylation with inhibitor treatment (top panel), SD and SxE sites showed an enrichment of 25% each.

We queried the data for the sites with the largest drug-induced change, and we retrieved a phosphorylation site on BSND with local sequence YYGLPDpSPGNPLP (S289). This site showed a nearly 10-fold decrease in phosphorylation upon treatment with either inhibitor (Figure 4A). We noted that the phosphorylation state of a second BSND phosphorylation

site S162, VVVHRGpSDENEGE, did not change, providing further evidence as to the specific effect of the inhibitor on S289 (Figure 4B). Moreover, the protein-level data for BSND did not show significant difference (Figure 4C) in the presence of the inhibitor, and as such revealed that the change in phosphorylation state was not an artifact of increased protein production. This finding was of particular interest as BSND, when mutated, caused altered chloride homeostasis and salt wasting [36]. Although not clearly understood functionally, BSND may be inactivated by tyrosine phosphorylation [36].

In addition to comparing the similarity of both drugs' effects, we also compared the differences in the action of these two drugs. At least in kidney tissue, these differences were very subtle. In total, 11 phosphorylation sites (Supplemental Figure 3) demonstrated statistically significant difference (corrected p-value < 0.05) in abundance when comparing the two drug treatments. Phosphosites significantly up-regulated in mice treated with GSK1120212 included P2ry2-329, Zc3hc1-343, C2cd2l-411, Traf4-426, Tjp1-617, and Hsd17b8-58, while those significantly up-regulated in mice treated with PD0325901 included Kiaa1543-830, Vps13d-1756, Agps-57, Eif4g1-1217, and Ttc15-313. Of these proteins, only two have some evidence supporting implications in kidney dysfunction but not specifically edema, both of which have a phosphorylation site that is up-regulated in the GSK1120212-treated mice. Tjp1 (tight junction protein ZO-1) is located on cytoplasmic membrane surface of intercellular tight junction which may transduce signals required for tight junction assembly stabilizing junctions [37]. The disruption of tight junctions have a role in chronic kidney disease [38]. Similarly, P2ry2 (purinoceptor 2) is a receptor for ATP and UTP that is coupled to G-proteins and has a role in the activation of a phosphatidylinositol-calcium second messenger system [39] which affects renal tubular transport [40].

Other proteins with statistically significant differences in phosphorylation events between the two drugs have many different cellular functions. Several of these proteins, including the aforementioned Tjp1 and P2ry2, were membrane or membrane-associated proteins. Ttc15 (trafficking protein particle complex subunit 12) may be involved in endoplasmic reticulum to Golgi apparatus trafficking at a very early stage [41]. Likewise, Vps13d (Vacuolar protein sorting-associated protein 13D) is involved in trafficking of membrane proteins in the trans-Golgi network [42]. C2cd2l (C2 domain-containing protein 2) is an integral membrane protein which has not been extensively studied [43]. Many of these membrane proteins act in signal transduction, as does Traf4 (TNF receptor-associated factor 4) which is an adapter protein and signal transducer that links members of the tumor necrosis factor receptor (TNFR) family thereby mediating signal transduction to different signaling pathways (e.g., NF-kappa-B and JNK [44]. Similarly, Kiaa1543 (Calmodulin-regulated spectrin-associated protein 3) is known to regulate the nucleation and the polymerization of microtubules [45]. Other proteins are involved in cell cycle and cell division. Zc3hc1 (Zinc Finger, C3HC-Type Containing 1) an F-box-containing protein that is a component of an SCF-type E3 ubiquitin ligase complex regulating the onset of cell division. [46]. Eif4g1-1217 Eukaryotic translation initiation factor 4 gamma 1 Component of the protein complex eIF4F, which is involved in the recognition of the mRNA cap, ATP-dependent unwinding of 5'-terminal secondary structure and recruitment of mRNA to the ribosome involved in the recognition of

the mRNA cap, ATP-dependent unwinding of 5'-terminal secondary structure [47, 48]. Organelle specific proteins were also identified in differentially phosphorylated states. Agps (alkyldihydroxyacetonephosphate synthase) is a peroxisomal protein that catalyzes the exchange of an acyl for a long-chain alkyl group and the formation of the ether bond in the biosynthesis of ether phospholipids [49]. Hsd17b8 (estradiol 17-beta-dehydrogenase 8 NAD-dependent 17-beta-hydroxysteroid dehydrogenase) is a mitochondrial protein that has a role in the biosynthesis of fatty acids in mitochondria [50]. The role of these proteins in edema and kidney dysfunction in relation to the differences in the downstream or off-target effects of these drugs is currently not completely understood and further study will enhance current knowledge concerning the differences in effects between these two drugs.

### 3.3 Phosphotyrosine enrichment showed a decrease in phosphorylation of MAPK1 and MAPK3

We enriched for phosphotyrosine-containing peptides via immunoprecipitation with an anti-phosphotyrosine antibody to interrogate deeper the phosphoproteomic alterations of these MEK inhibitors on kidney function. Of the 592 phosphotyrosine features identified, 16 showed significantly altered phosphorylation, including MAPK1 (ERK2) and MAPK3 (ERK1) (Figure 5). MEK inhibition blocks ERK1/2 phosphorylation, the targets for the MEK kinases. These ERK kinases are mitogen-activated protein kinases belonging to the CMGC (CDK/MAPK/GSK3/CLK) kinase group [51]. Typically these kinases require the target serine or threonine residues to be followed by a less bulky amino acid, usually proline, and thus are commonly referred to as proline-directed kinases [52]. As MAPK1 and MAPK3 phosphorylate SP residues, such a result was consistent with our previous motif analysis showing greater than 25-fold enrichment in SP motifs in a cluster of phosphopeptides in which phosphorylation decreased when the mice were treated with either inhibitor (Figure 3B). It was worth noting that the MAPK1 and MAPK3 phosphopeptides were not identified when TiO<sub>2</sub> enrichment alone was used, and thereby under the experimental conditions herein were identified only with phosphotyrosine immunoprecipitation.

## 4. Discussion

We developed a platform based upon the analysis of 10 samples simultaneously (3x3+1 TMT10-plex experiment) to characterize the effects of two MEK inhibitor drugs (GSK1120212 and PD0325901) across 3 tissue types. We observed very few changes at the protein level in the three tissues. Focusing on kidney tissue, we investigated phosphoproteomic alterations. More than 10,000 sites were quantified from the TiO<sub>2</sub> enriched samples, and an additional 592 sites were profiled after antibody-based phosphotyrosine enrichment. K-means clustering analysis revealed a decrease in phosphorylation of SP and PxSP motifs, and an increase in phosphorylation of the more acidic motifs, SD and SxE, with inhibitor treatment. We focused our analysis on the kidney to understand better the fluid retention phenotype resulting from the treatment of our mouse model with the inhibitors. We observed a significant decrease in the phosphorylation of a PxSP motif in a BSND (Bartter syndrome with sensorineural deafness) peptide (BSND-S289). Phosphotyrosine enrichment of the kidney tissue revealed a decrease in the

phosphorylation of MAPK1 and MAPK3 residues. The inactivation of these kinases may be involved in the mechanism that results in decreased phosphorylation of BSND-S289, which has a PxSP motif and thus is a common target of MAPK1 and MAPK3.

Fluid retention, more specifically, edema, has been identified as an adverse effect in clinical trials of both GSK1120212 and PD0325901 [5, 9, 10, 14]. As noted above, one of the most significantly altered phosphorylation sites in our study is localized on the BSND protein [36]. This protein is an essential beta subunit of CLC chloride channels and is localized to the basolateral membranes of renal tubules [53, 54]. Renal dysfunction is associated with BSND expression [55], and alterations in the protein have been associated with Bartter syndrome [56]. The BSND phosphorylation site (S289) with motif YYGLPDpSPGNPLP shows approximately a 10-fold decrease in phosphorylation upon treatment with either inhibitor. We also observe that the protein level of BSND does not change significantly, nor does the phosphorylation state of a second BSND phosphorylation site S162 (Figure 4). It is noteworthy that although this PxSP site is conserved in several mammalian species, this site is not conserved in primates (Supplemental Figure 4). Although these drugs have a profound effect on BSND phosphorylation at S162 and may result in aberrant downstream effects in mice, the event is not preserved in humans. Further studies are needed to investigate the global implications of the effects of GSK1120212 and PD0325901 on this phosphorylation site in mice with respect to its absence in humans.

In addition, we identified peptides from Solute carrier family 12 member 3 (Slc12a3), a known interacting partner of BSND [57]. Of particular interest is the phosphorylation site with residue S124, which has been discovered recently [58] and has been characterized extensively in rats [59]. This phosphorylation site, DETGTNpSEKSPGE, unlike BSND-S289, shows an increase in phosphorylation upon treatment with the inhibitors, as illustrated in Figure 3. Moreover, in contrast to BSND, the S124 site on Slc12a3 is conserved in humans and therefore may be a target of these inhibitors that is common in both species. The relationship between BSND, Slc12a3, and the associated phosphorylation events is currently not well understood and targeted studies will be needed to elucidate the mechanisms of action.

Here we present one of the first studies using a TMT10-plex system, which expands the potential of commercially available isobaric tag multiplexing reagents which up until recently allowed a maximum of 8 channels [27, 60]. First, throughput is increased as multiple samples may be analyzed simultaneously, resulting in reduced instrument time and associated costs. Second, fewer missing values are observed, as is common in metabolic labeling, because the isobaric peptides from different samples are isolated and fragmented together to produce the reporter ions. And third, multiple comparisons may be performed in a single experiment, such that statistical significance may be assessed while minimizing differences due to instrumental conditions. A major advantage of our strategy over the commonly-used TMT6-plex strategy is the ability to more confidently apply statistical methods (i.e., t-tests and ANOVA) to ternary comparisons in a single experiment. We expect higher order multiplexing reagents to highlight further these advantages.

The importance of enriching for phosphotyrosine-containing peptides to achieve a greater depth of low abundant phosphorylation sites using our workflow is emphasized by our identification of MAPK1 and MAPK3 phosphopeptides following phosphotyrosine immunoprecipitation. From these proteins, two phosphopeptides were detected only via the pY IP and were not identified by TiO<sub>2</sub> enrichment alone. These phosphopeptides contained both a tyrosine and a threonine, however only the tyrosine on this peptide was phosphorylated. Phosphorylation of tyrosine residues is a rare event, comprising approximately 0.05 – 1.8% of total phosphorylation sites in the cell [61]. We were able only to detect the direct targets of MEK through phosphotyrosine affinity isolation, suggesting that phosphotyrosine analysis is compatible with the TMT10-plex pipeline.

We compared the effects of two MEK inhibitors to vehicle treatment to study the global effects of these inhibitors on a mouse model. In general, both inhibitors affect target sites in kidney tissue in a similar manner as per the direction of changes in phosphorylation events. Such would imply a high degree of on-target versus off-target effects although these two inhibitors differ substantially in their chemical structures (Figure 1). Further phosphorylation-based studies on the other tissues, e.g. liver and pancreas, may provide added insight into the differences in the off-target effects of these drugs.

Future experiments may also extend the strategy that we have outlined herein. For example, differences in the effects of the inhibitors to each other at the protein and phosphoprotein level may elucidate the specific targets of each inhibitor. In addition, one can expand the number of tissues investigated. Experiments could also be designed such that 10 tissues are compared in a single experiment and multiple 10-plexes are analyzed as biological replicates. Essentially, TMT 10-plex offers tremendous flexibility for robust proteome and phosphoproteome analysis for virtually any biological system.

In conclusion, our data highlight the use of higher order TMT-based multiplexing to interrogate the global proteomes and phosphoproteomes of multiple tissues in an unbiased manner towards discovering potential functional alterations. These data may provide insight into the phenotypic differences resulting from MEK inhibitor treatments. Further bioinformatic analysis of these data may yield insights into the mechanisms modulated by GSK1120212 and PD0325901. For example, the enrichment of SP sites may implicate cyclin dependent kinases (CDK) as having a role on alterations in cell signaling due to drug treatment. The 3x3+1 strategy permits the comparison of 3 different states in triplicate, thereby allowing for statistical analysis within each experiment, and the ability to compare data across multiple experiments with the tenth channel. This versatile strategy can be applied to virtually any organism, organ, or disease model, making it a powerful multiplexing method. Upon the introduction of higher-plexed isobaric labeling, a greater number of replicates or conditions could be analyzed in a single experiment resulting in improved statistical analyses.

## Supplementary Material

Refer to Web version on PubMed Central for supplementary material.

## Acknowledgments

We would like to acknowledge the generous assistance of Dr. Joseph Bonventre for thoughtful discussions. In addition, we would like to thank all the members of the Gygi lab, in particular Dr. Mark P. Jedrychowski, for technical assistance and insights. This work was funded in part by NIH/NIDDK grant: K01DK098285 (JP) and K01DK093638 (AB).

## Abbreviations

<b>BSND</b>	Bartter syndrome, infantile, with sensorineural deafness
<b>FDR</b>	false discovery rate
<b>BpRP</b>	basic pH reversed-phase chromatography
<b>pY IP</b>	phosphotyrosine immunoprecipitation
<b>TMT</b>	tandem mass tag

## References

- Dayon L, Hainard A, Licker V, Turck N, et al. Relative quantification of proteins in human cerebrospinal fluids by MS/MS using 6-plex isobaric tags. *Anal Chem.* 2008; 80:2921–2931. [PubMed: 18312001]
- Thompson A, Schafer J, Kuhn K, Kienle S, et al. Tandem mass tags: a novel quantification strategy for comparative analysis of complex protein mixtures by MS/MS. *Analytical chemistry.* 2003; 75:1895–1904. [PubMed: 12713048]
- Ross PL, Huang YN, Marchese JN, Williamson B, et al. Multiplexed protein quantitation in *Saccharomyces cerevisiae* using amine-reactive isobaric tagging reagents. *Molecular & cellular proteomics : MCP.* 2004; 3:1154–1169. [PubMed: 15385600]
- Wang D, Boerner SA, Winkler JD, LoRusso PM. Clinical experience of MEK inhibitors in cancer therapy. *Biochim Biophys Acta.* 2007; 1773:1248–1255. [PubMed: 17194493]
- Kim KB, Kefford R, Pavlick AC, Infante JR, et al. Phase II study of the MEK1/MEK2 inhibitor Trametinib in patients with metastatic BRAF-mutant cutaneous melanoma previously treated with or without a BRAF inhibitor. *Journal of clinical oncology : official journal of the American Society of Clinical Oncology.* 2013; 31:482–489. [PubMed: 23248257]
- Lawrence M, Jivan A, Shao C, Duan L, et al. The roles of MAPKs in disease. *Cell research.* 2008; 18:436–442. [PubMed: 18347614]
- Hommel D, Peppelenbosch M, van Deventer S. Mitogen activated protein (MAP) kinase signal transduction pathways and novel anti-inflammatory targets. *Gut.* 2003; 52:144–151. [PubMed: 12477778]
- Akinleye A, Furqan M, Mukhi N, Ravella P, Liu D. MEK and the inhibitors: from bench to bedside. *Journal of hematology & oncology.* 2013; 6:27. [PubMed: 23587417]
- Boasberg PD, Redfern CH, Daniels GA, Bodkin D, et al. Pilot study of PD-0325901 in previously treated patients with advanced melanoma, breast cancer, and colon cancer. *Cancer chemotherapy and pharmacology.* 2011; 68:547–552. [PubMed: 21516509]
- LoRusso PM, Krishnamurthi SS, Rinehart JJ, Nabell LM, et al. Phase I pharmacokinetic and pharmacodynamic study of the oral MAPK/ERK kinase inhibitor PD-0325901 in patients with advanced cancers. *Clin Cancer Res.* 2010; 16:1924–1937. [PubMed: 20215549]
- Iverson C, Larson G, Lai C, Yeh LT, et al. RDEA119/BAY 869766: a potent, selective, allosteric inhibitor of MEK1/2 for the treatment of cancer. *Cancer Res.* 2009; 69:6839–6847. [PubMed: 19706763]
- Huang W, Yang AH, Matsumoto D, Collette W, et al. PD0325901, a mitogen-activated protein kinase kinase inhibitor, produces ocular toxicity in a rabbit animal model of retinal vein occlusion.

Journal of ocular pharmacology and therapeutics : the official journal of the Association for Ocular Pharmacology and Therapeutics. 2009; 25:519–530.

13. Yao, S. US Food and Drug Administration. FDA; 2013. <http://www.fda.gov>
14. Falchook GS, Lewis KD, Infante JR, Gordon MS, et al. Activity of the oral MEK inhibitor trametinib in patients with advanced melanoma: a phase 1 dose-escalation trial. *The lancet oncology*. 2012; 13:782–789. [PubMed: 22805292]
15. Kumar, V.; Abbas, AK.; Fausto, N.; Robbins, SL.; Cotran, RS. Robbins and Cotran pathologic basis of disease. Elsevier Saunders; Philadelphia: 2005.
16. Friedman JM, Halaas JL. Leptin and the regulation of body weight in mammals. *Nature*. 1998; 395:763–770. [PubMed: 9796811]
17. Zhang Y, Proenca R, Maffei M, Barone M, et al. Positional cloning of the mouse obese gene and its human homologue. *Nature*. 1994; 372:425–432. [PubMed: 7984236]
18. Ingalls AM, Dickie MM, Snell GD. Obese, a new mutation in the house mouse. *The Journal of heredity*. 1950; 41:317–318. [PubMed: 14824537]
19. Jiang ZY, Lin YW, Clemont A, Feener EP, et al. Characterization of selective resistance to insulin signaling in the vasculature of obese Zucker (fa/fa) rats. *J Clin Invest*. 1999; 104:447–457. [PubMed: 10449437]
20. Wessel D, Flügge U. A method for the quantitative recovery of protein in dilute solution in the presence of detergents and lipids. *Anal Biochem*. 1984; 138:141–143. [PubMed: 6731838]
21. Kettenbach A, Gerber S. Rapid and reproducible single-stage phosphopeptide enrichment of complex peptide mixtures: application to general and phosphotyrosine-specific phosphoproteomics experiments. *Anal Chem*. 2011; 83:7635–7644. [PubMed: 21899308]
22. Ting L, Rad R, Gygi S, Haas W. MS3 eliminates ratio distortion in isobaric multiplexed quantitative proteomics. *Nat Methods*. 2011; 8:937–940. [PubMed: 21963607]
23. McAlister GC, Nusinow DP, Jedrychowski MP, Wuhr M, et al. MultiNotch MS3 Enables Accurate, Sensitive, and Multiplexed Detection of Differential Expression across Cancer Cell Line Proteomes. *Analytical chemistry*. 2014; 86:7150–7158. [PubMed: 24927332]
24. Elias JE, Gygi SP. Target-decoy search strategy for mass spectrometry-based proteomics. *Methods Mol Biol*. 2010; 604:55–71. [PubMed: 20013364]
25. Elias JE, Gygi SP. Target-decoy search strategy for increased confidence in large-scale protein identifications by mass spectrometry. *Nat Methods*. 2007; 4:207–214. [PubMed: 17327847]
26. Huttlin EL, Jedrychowski MP, Elias JE, Goswami T, et al. A tissue-specific atlas of mouse protein phosphorylation and expression. *Cell*. 2010; 143:1174–1189. [PubMed: 21183079]
27. McAlister GC, Huttlin EL, Haas W, Ting L, et al. Increasing the multiplexing capacity of TMTs using reporter ion isotopologues with isobaric masses. *Analytical chemistry*. 2012; 84:7469–7478. [PubMed: 22880955]
28. Benjamini Y, Hochberg Y. Controlling the false discovery rate - a practical and powerful approach to multiple testing. *Journal of the Royal Statistical Society Series B-Methodological*. 1995; 57:289–300.
29. Beausoleil SA, Villen J, Gerber SA, Rush J, Gygi SP. A probability-based approach for high-throughput protein phosphorylation analysis and site localization. *Nat Biotechnol*. 2006; 24:1285–1292. [PubMed: 16964243]
30. Schwartz D, Gygi SP. An iterative statistical approach to the identification of protein phosphorylation motifs from large-scale data sets. *Nat Biotechnol*. 2005; 23:1391–1398. [PubMed: 16273072]
31. Crooks GE, Hon G, Chandonia JM, Brenner SE. WebLogo: a sequence logo generator. *Genome research*. 2004; 14:1188–1190. [PubMed: 15173120]
32. Paulo JA, Kadiyala V, Lee LS, Banks PA, et al. Proteomic analysis (GeLC-MS/MS) of ePFT-collected pancreatic fluid in chronic pancreatitis. *J Proteome Res*. 2012; 11:1897–1912. [PubMed: 22243521]
33. Fletcher PL Jr, Fletcher MD, Weninger K, Anderson TE, Martin BM. Vesicle-associated membrane protein (VAMP) cleavage by a new metalloprotease from the Brazilian scorpion *Tityus serrulatus*. *J Biol Chem*. 2010; 285:7405–7416. [PubMed: 20026600]

34. Seyberth HW, Schlingmann KP. Bartter- and Gitelman-like syndromes: salt-losing tubulopathies with loop or DCT defects. *Pediatr Nephrol.* 2011; 26:1789–1802. [PubMed: 21503667]
35. Chou, MF.; Schwartz, D. Biological sequence motif discovery using motif-x. In: Baxeavanis, Andreas D., et al., editors. *Current protocols in bioinformatics / editorial board.* Vol. Chapter 13. 2011. p. 15-24.
36. Estevez R, Boettger T, Stein V, Birkenhager R, et al. Barttin is a Cl<sup>-</sup> channel beta-subunit crucial for renal Cl<sup>-</sup> reabsorption and inner ear K<sup>+</sup> secretion. *Nature.* 2001; 414:558–561. [PubMed: 11734858]
37. Li X, Ionescu AV, Lynn BD, Lu S, et al. Connexin47, connexin29 and connexin32 co-expression in oligodendrocytes and Cx47 association with zonula occludens-1 (ZO-1) in mouse brain. *Neuroscience.* 2004; 126:611–630. [PubMed: 15183511]
38. Vaziri ND, Yuan J, Nazertehrani S, Ni Z, Liu S. Chronic kidney disease causes disruption of gastric and small intestinal epithelial tight junction. *American journal of nephrology.* 2013; 38:99–103. [PubMed: 23887095]
39. Enomoto K, Furuya K, Moore RC, Yamagishi S, et al. Expression cloning and signal transduction pathway of P2U receptor in mammary tumor cells. *Biological signals.* 1996; 5:9–21. [PubMed: 8739319]
40. Praetorius HA, Leipziger J. Intrarenal purinergic signaling in the control of renal tubular transport. *Annual review of physiology.* 2010; 72:377–393.
41. Villen J, Beausoleil SA, Gerber SA, Gygi SP. Large-scale phosphorylation analysis of mouse liver. *Proc Natl Acad Sci U S A.* 2007; 104:1488–1493. [PubMed: 17242355]
42. Andersson B, Wentland MA, Ricafrente JY, Liu W, Gibbs RA. A “double adaptor” method for improved shotgun library construction. *Anal Biochem.* 1996; 236:107–113. [PubMed: 8619474]
43. Katoh M, Katoh M. Identification and characterization of TMEM24 family genes in silico. *International journal of oncology.* 2004; 25:759–764. [PubMed: 15289880]
44. Shiels H, Li X, Schumacker PT, Maltepe E, et al. TRAF4 deficiency leads to tracheal malformation with resulting alterations in air flow to the lungs. *Am J Pathol.* 2000; 157:679–688. [PubMed: 10934170]
45. Tanaka N, Meng W, Nagae S, Takeichi M. Nezha/CAMSAP3 and CAMSAP2 cooperate in epithelial-specific organization of noncentrosomal microtubules. *Proc Natl Acad Sci U S A.* 2012; 109:20029–20034. [PubMed: 23169647]
46. Church DM, Goodstadt L, Hillier LW, Zody MC, et al. Lineage-specific biology revealed by a finished genome assembly of the mouse. *PLoS biology.* 2009; 7:e1000112. [PubMed: 19468303]
47. Pyronnet S, Imataka H, Gingras AC, Fukunaga R, et al. Human eukaryotic translation initiation factor 4G (eIF4G) recruits mnk1 to phosphorylate eIF4E. *Embo J.* 1999; 18:270–279. [PubMed: 9878069]
48. Imataka H, Sonenberg N. Human eukaryotic translation initiation factor 4G (eIF4G) possesses two separate and independent binding sites for eIF4A. *Mol Cell Biol.* 1997; 17:6940–6947. [PubMed: 9372926]
49. Brown AJ, Snyder F. Alkyldihydroxyacetone-P synthase. Solubilization, partial purification, new assay method, and evidence for a ping-pong mechanism. *J Biol Chem.* 1982; 257:8835–8839. [PubMed: 7096336]
50. Ando A, Kikuti YY, Shigenari A, Kawata H, et al. cDNA cloning of the human homologues of the mouse Ke4 and Ke6 genes at the centromeric end of the human MHC region. *Genomics.* 1996; 35:600–602. [PubMed: 8812499]
51. Manning G, Whyte DB, Martinez R, Hunter T, Sudarsanam S. The protein kinase complement of the human genome. *Science.* 2002; 298:1912–1934. [PubMed: 12471243]
52. Garai Á, Zeke A, Gógl G, Tör I, et al. Specificity of linear motifs that bind to a common mitogen-activated protein kinase docking groove. *Science signaling.* 2012; 5
53. Lang F. Modulation of Cl<sup>-</sup>-K<sup>+</sup> channel function by the accessory subunit barttin. *J Am Soc Nephrol.* 2010; 21:1238–1239. [PubMed: 20595683]
54. Kramer BK, Bergler T, Stoelcker B, Waldegger S. Mechanisms of Disease: the kidney-specific chloride channels ClCKA and ClCKB, the Barttin subunit, and their clinical relevance. *Nature clinical practice. Nephrology.* 2008; 4:38–46.

55. Park CW, Lim JH, Youn DY, Chung S, et al. Renal dysfunction and barttin expression in Bartter syndrome Type IV associated with a G47R mutation in BSND in a family. *Clinical nephrology*. 2011; 75(Suppl 1):69–74. [PubMed: 21269598]
56. Fischer M, Janssen AG, Fahlke C. Barttin activates ClC-K channel function by modulating gating. *J Am Soc Nephrol*. 2010; 21:1281–1289. [PubMed: 20538786]
57. Birkenhager R, Otto E, Schurmann MJ, Vollmer M, et al. Mutation of BSND causes Bartter syndrome with sensorineural deafness and kidney failure. *Nat Genet*. 2001; 29:310–314. [PubMed: 11687798]
58. Feric M, Zhao B, Hoffert JD, Pisitkun T, Knepper MA. Large-scale phosphoproteomic analysis of membrane proteins in renal proximal and distal tubule. *American journal of physiology. Cell physiology*. 2011; 300:C755–770. [PubMed: 21209370]
59. Rosenbaek LL, Assentoft M, Pedersen NB, MacAulay N, Fenton RA. Characterization of a novel phosphorylation site in the sodium-chloride cotransporter, NCC. *The Journal of physiology*. 2012; 590:6121–6139. [PubMed: 22966159]
60. Werner T, Becher I, Sweetman G, Doce C, et al. High-resolution enabled TMT 8-plexing. *Anal Chem*. 2012; 84:7188–7194. [PubMed: 22881393]
61. Hunter T, Sefton BM. Transforming gene product of Rous sarcoma virus phosphorylates tyrosine. *Proc Natl Acad Sci U S A*. 1980; 77:1311–1315. [PubMed: 6246487]

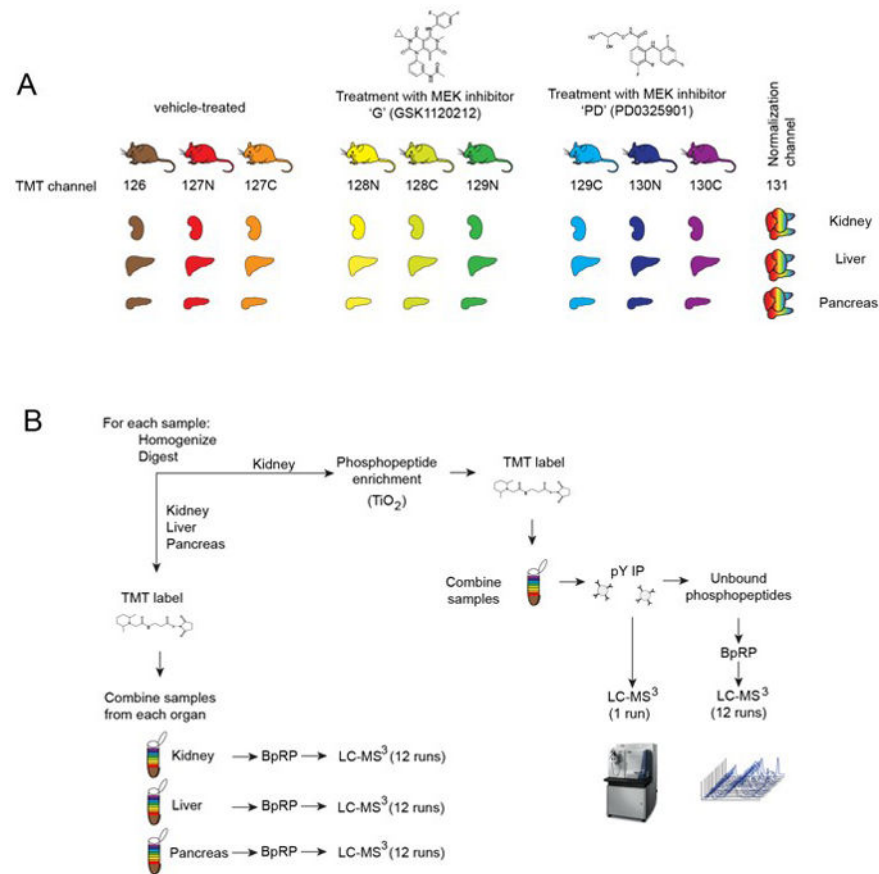


**Figure 1. Experimental overview using TMT10-plex quantitation**

**A)** The 3x3+1 strategy consists of triplicate analyses of vehicle-, GSK1120212-, and PD0325901-treated mice plus a cross-over channel comprising a mix of all samples allowing for the comparison across three separate TMT experiments and thus between tissue types and inhibitor treatments. **B)** Experimental details. Mouse tissues were harvested and proteolyzed. For protein expression profiling, peptides were labeled with TMT reagents and then combined as shown in Panel A. Labeled peptides were separated by basic pH reverse-phase (BpRP) chromatography with fraction collection. Fractions (12) were analyzed by an LC-MS<sup>3</sup> method using a 3-hr gradient. For phosphorylation analysis, two different experiments were collected. First, phosphopeptides were first enriched using TiO<sub>2</sub> and then labeled with TMT reagents. Second, phosphotyrosine-containing peptides were enriched via anti-phosphotyrosine antibodies. The unbound phosphopeptide fraction was analyzed via BpRP chromatography (12 fractions) for general phosphorylation. The affinity isolated phosphotyrosine sample was analyzed by a single 3-hr LC-MS<sup>3</sup> analysis.

A.

Tissue	Total peptides	Unique peptides	Proteins quantified
kidney	88,192	45,620	5908
liver	84,748	39,279	5819
pancreas	76,782	41,575	5644

B.

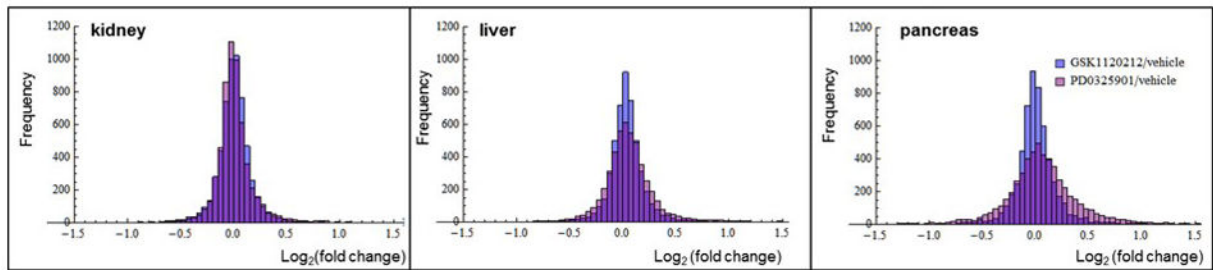


**Figure 2. Summary of protein expression data**

**A)** Summary of total peptides, unique peptides and proteins quantified in each tissue at <1% FDR. **B)** Distributions of  $\log_2$ -transformed fold change ratios for three tissues comparing the drug treatment to control. V, vehicle; G, GSK1120212; PD, PD0325901.

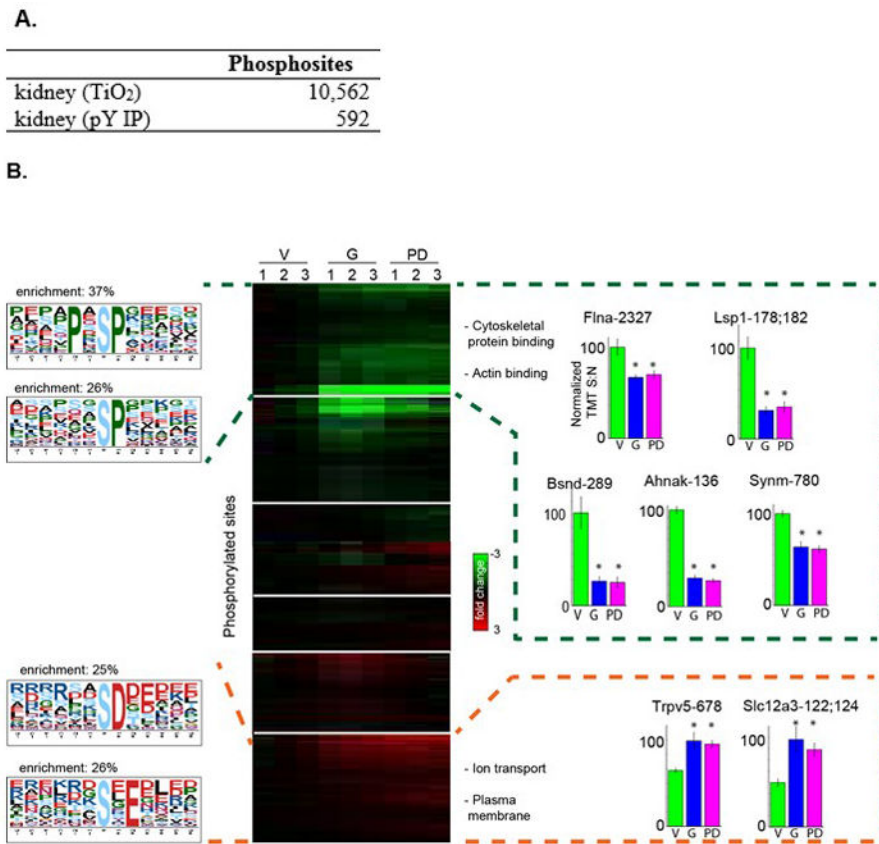


**Figure 3. Summary of TiO<sub>2</sub> phosphorylation enrichment data**

**A)** Phosphopeptides identified by TiO<sub>2</sub> (titanium dioxide enrichment) and pY IP (phosphotyrosine immunoprecipitation). **B)** Heat map of clustered phosphorylation changes in kidney tissue. K-means clustering of significantly changing sites from kidney tissue of mice treated with vehicle, GSK1120212, and PD0325901. Gene ontology (GO) enrichment terms for each of the clusters are shown alongside the clusters, as are bar charts showing effects of inhibitor treatments for representative sites. Motifs that are enriched for the inhibitor treatments are illustrated on the left. V, vehicle; G, GSK1120212; PD, PD0325901; SN, signal-to-noise; \*, p-value < 0.05 versus vehicle as determined via ANOVA and post-hoc Tukey's test.

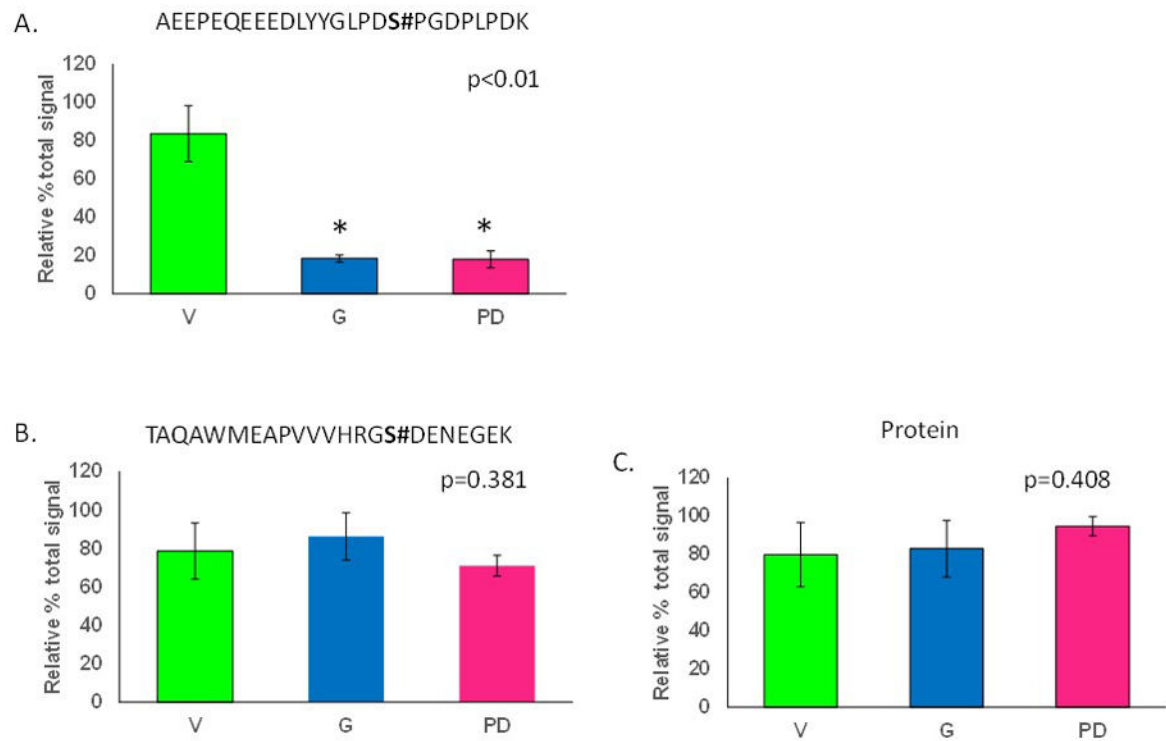


**Figure 4. Protein expression and phosphorylation analysis for BSND protein**

**A)** Relative abundance of site S298 showing decreased phosphorylation upon either drug treatment. **B)** Site S162 phosphorylation shows no alteration in phosphorylation levels. **C)** Normalized TMT signal to noise ratio (S/N) for BSND protein expression does not change. \*, p-value<0.05 versus vehicle as determined via ANOVA and post-hoc Tukey's test.

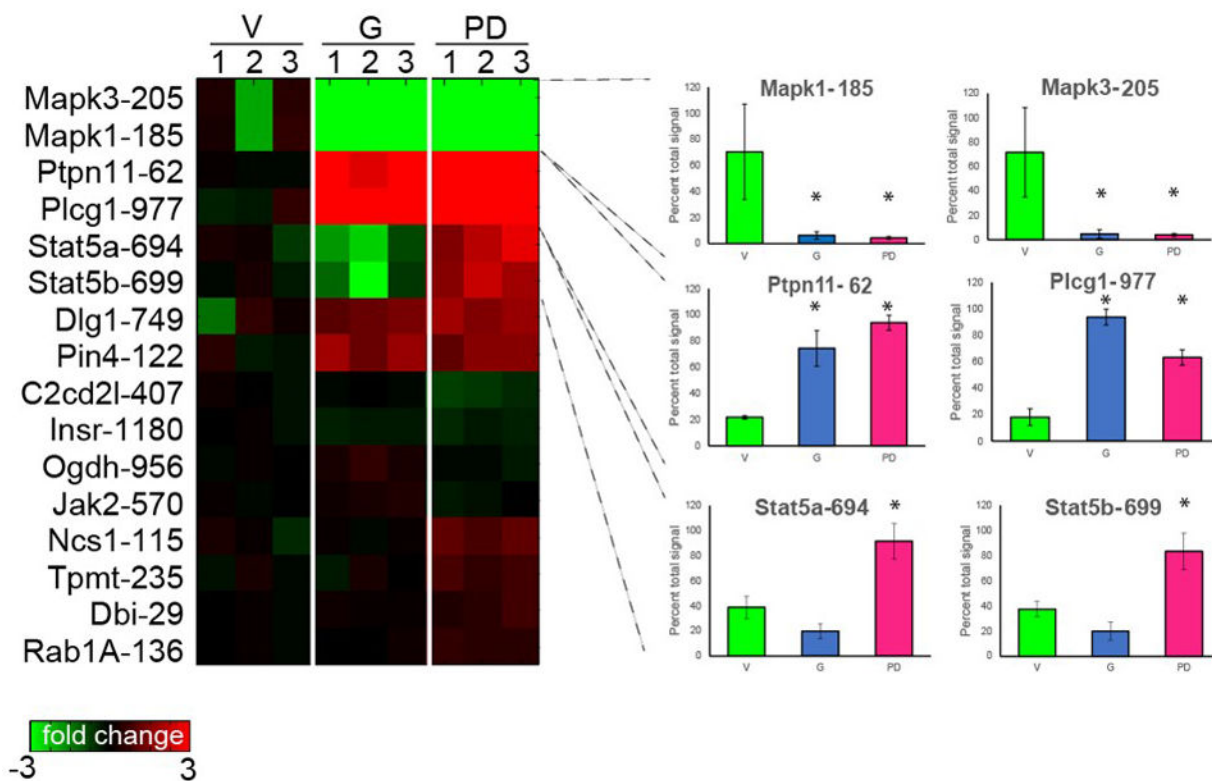


**Figure 5. Enrichment of kidney phosphotyrosine (pY)-containing peptides via immunoprecipitation**

Left: Heat map of significant phosphotyrosine-containing peptide changes following enrichment. Right: Histograms of TMT signal-to-noise (SN) intensity for example phosphotyrosine sites. V, vehicle; G, GSK1120212; PD, PD0325901; \*, p-value<0.05 versus vehicle control as determined via ANOVA and post-hoc Tukey’s test.